Biomedical Signal Processing and Control 86 (2023) 105319

Contents lists available at ScienceDirect

Biomedical Signal Processing and Control

journal homepage: www.elsevier.com/locate/bspc

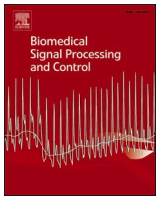

Optimal lung cancer detection based on CNN optimized and improved Snake optimization algorithm

Chaohua Yan [a,*], Navid Razmjooy [b,c,d,*]

[a] School of Digital Media and Art Design, Nanyang Institute of Technology, Nanyang, Henan, 473004, China
[b] Young Researchers and Elite Club, Ardabil Branch, Islamic Azad University, Ardabil, Iran
[c] Department of Computer Science and Engineering, Division of Research and Innovation, Saveetha School of Engineering, SIMATS, Chennai 602105, Tamil Nadu, India
[d] College of Technical Engineering, The Islamic University, Najaf, Iraq

ARTICLE INFO

Keywords:
Lung cancer
Automatic diagnosis
Convolutional neural networks
improved version of the Snake optimization algorithm

ABSTRACT

Lung cancer is an ailment that lessens the patient's capability to breathe because of the excessive spread of lung tissue cells. The cancer spreads after genetic damage to DNA. This genetic damage results in the excessive distribution and proliferation of cells, which ultimately creates a mass called a tumor. Using automatic machine vision techniques is an effective method for lung cancer detection. A novel lung cancer detection methodology for the automatic identification of lung cancer in CT images is proposed in this work This technique is developed by convolutional neural networks (CNNs). Here, the lung cancer images are first preprocessed before being included in the designed CNN. To provide optimal CNN design, a novel modified version of Snake Optimizer is designed and applied to the CNN structure. The proposed model is then tested against the "IQ-OTH/NCCD-Lung Cancer Dataset". This strategy is also validated by comparing it with some different published methods in the literature. The findings demonstrated that the offered strategy outperformed the others.

1. Introduction

One of the deadliest types of cancer is Lung cancer, with more victims than breast and prostate cancer combined. Every year, approximately 1.8 million cases of this kind of cancer have been identified worldwide, with 1.5 million people dying as a result [1]. Lung cancer accounts for one in every five cancer fatalities [2]. Early diagnosis of the condition, according to studies, is the most efficient option to improve a person's life expectancy [3].

Lung cancer is most common in the elderly [4]. Almost two-thirds of lung cancer patients are over the age of 65, with less than 2% being under the age of 45. Patients are typically 70 years old. The incidence of lung cancer is influenced by a variety of factors, including age, gender, genetics, lifestyle choices, and environmental exposures. Lung cancer affects one out of every fourteen men and one out of every seventeen women [5]. One reason why lung cancer affects more men than women is that historically, men have had higher rates of smoking, which is a major risk factor for the disease. However, as smoking rates have decreased in recent decades, the incidence of lung cancer in women has also increased. Other risk factors for lung cancer include exposure to secondhand smoke, air pollution, radon, and occupational exposures to certain chemicals and substances. Additionally, some genetic factors may also increase an individual's risk of developing lung cancer. In general, the development of lung cancer is complex and multifactorial, and further research is needed to fully understand the underlying mechanisms and risk factors involved. The vast majority of cancer-related death is caused by Lung cancer, killing about 1.8 million people globally each year. However, a vast number of lung cancer cases are discovered late, resulting in the least effective treatment [6].

CT scans, or computed tomography (CT) scans, can reveal the features of malignant cells, and a biopsy or surgery following a Computed tomography can prove the tumor's malignancy [7]. However, each scan requires a professional radiologist to evaluate 300 images to discover critical symptoms of lung cancer, which can be subtle and small [8].

That's why researchers are hopeful about the use of artificial intelligence in the lung cancer scanning technique, due to the fact that it speeds up the diagnosis process and potentially detects patients at an early, treatable stage [9]. The new artificial intelligence technology can help in the early detection of lung cancer and has so far been effective in detecting 97% of tumors [8]. Malignant lung masses can be detected by machine learning faster than radiologists. The machine learning system can give an image evaluation system capable of detecting lung cancer in

* Corresponding authors.
E-mail addresses: yanchaohua@126.com (C. Yan), nrazmjooy@gmail.com (N. Razmjooy).

https://doi.org/10.1016/j.bspc.2023.105319
Received 19 April 2023; Received in revised form 4 July 2023; Accepted 31 July 2023
Available online 9 August 2023

real-time [10]. The use of machine learning models for medical image analysis has shown great promise in recent years, with many studies demonstrating their ability to accurately detect and classify various diseases and conditions. In the case of lung cancer detection, several studies have compared the performance of machine-learning models to that of human radiologists, with some showing that the models can outperform the experts in certain circumstances. While these studies demonstrate the potential of machine learning models for improving the accuracy and efficiency of lung cancer detection, it is important to note that the models are not intended to replace radiologists or other medical professionals. Rather, they can serve as a valuable tool to assist in the interpretation of medical images and to help identify potential cases for further evaluation and diagnosis.

Doctors can now read CT scan images more clearly because of artificial intelligence. By finding patterns and analyzing images, this technique can make it easier to comprehend scans connected to MRI, X-ray, and microscopic slides. The researchers initially fed the data from the medical photos into the machine learning techniques [11]. The computers then learn to identify patterns associated with each condition and diagnose the type of sickness by following an algorithm or a set of instructions. Obviously, the greater the quantity of data points, the more precise the disease diagnosis.

The employment of an optimization technique to deal with artificial neural network constraints can have a substantial influence on the system. To carry out the optimization, CT scans are employed. By correctly identifying the pictures, this approach produces more acceptable lung tumor outcomes. Much study has been conducted in this area, as can be seen in the list below.

Manoharan et al. [12] detected lung cancer by assessing the likelihood of malignancy and separating lung CT scan data automatically. To identify the lung nodules and diagnose the cancer cells, a computer-aided detection technique was devised. The primary goal of this research is to enable automatic picture processing and malignancy computation. The suggested model is tested in both internal and external nodules, with the findings displayed as response characteristics curves. The relationship between lung nodule size and cancer risk is complex and depends on a variety of factors, including nodule characteristics, smoking history, and other risk factors. While larger nodules may be more likely to be cancerous, the size of a nodule alone is not a definitive indicator of cancer risk [13].

Lakshmanaprabu et al. [14] demonstrated the best deep-learning technique for detecting lung cancer in CT scan data. A CT scan is employed for locating tumors and determining the extent of cancer in the body. The Optimal Deep Neural Network (ODNN) is utilized for CT scans and then an optimization process is implemented using the Improved GSO (Gravitational Search Optimizer) to classify lung cancer. According to the comparative results, the proposed classifier has around 94.5 percent accuracy, about 96 percent sensitivity, and 94 percent specificity.

Chakravarthy et al. [15] presented an improved probabilistic NN technique for the detection of lung cancer. Lung cancer is the most widespread kind in males and the 3rd most prevalent in females. Because lung cancer symptoms are only detected at an advanced phase, it is critical to predict the illness at an earlier phase using medical imaging tools. In this work, the goal is to present an automated categorization system for lung cancer at an early stage. The results show that the CCSA-based feature selection delivers an effective performance of 90% for the classification algorithm.

Shakeel et al. [16] used discrete AdaBoost optimized ensemble method generalized neural networks to detect lung cancer from biological data collection. Lung cancer affects the majority of people, primarily due to genetic alterations in the lungs' tissues. Smoking, alcohol, and exposure to hazardous gases can all be considered contributing factors. Although CAD systems in hospitals are capable of detecting lung cancer in its initial steps, obtaining the accuracy of cancer detection is challenging. The ELVIRA Biomedical Data Set Repository was used to collect lung biomedical data. The noise in the data was removed using the bin smoothing normalization procedure. The system's efficiency was assessed using a MATLAB experimental setting. It effectively classified normal and abnormal traits with high accuracy.

Toğaçar et al. [17] used an MRMR feature selection strategy with CNN to detect lung cancer on chest Computed tomography. Lung cancer is described by an uncontrollable growth of cells in the lung. Early diagnosis of malignant cells is critical in the lungs, which provide oxygen to the human body. Deep learning models LeNet, AlexNet, and VGG-16 are used in this work to detect lung tumors. The studies were conducted using an available dataset of Computed Tomography (CT) images. Convolutional neural networks (CNNs) were utilized in the experiment for feature extraction and classification. The highest efficient classification accuracy was 98.74 percent, attained by combining the AlexNet model and the NN classifier. The suggested model is a consistent diagnosis approach for detecting lung cancer utilizing chest CT data.

According to the published studies, some research regarding the automated detection of lung cancer utilizing image processing and machine vision has been introduced. We provide an enhanced approach system in the current study to help the system's correctness as much as feasible. The strategy, which uses a pipeline, yields the best outcomes for the dataset under study, as will be demonstrated.

The primary contribution of this study involves the introduction of a novel methodology for achieving optimal lung cancer detection. This is accomplished through the utilization of convolutional neural networks (CNNs) combined with an enhanced iteration of the Snake optimization algorithm. Through the integration of these two methodologies, the research attains notable progress in enhancing the precision and effectiveness of lung cancer detection in CT scans. The optimized convolutional neural network (CNN) is trained with the objective of acquiring knowledge about distinctive features related to lung cancer, thereby enhancing its ability to accurately classify novel images. The utilization of the modified Snake optimization algorithm is implemented to further optimize the design of the Convolutional Neural Network (CNN) model.

This contribution not only enhances the automated identification of lung cancer but also presents a streamlined and efficient approach that has the potential to save time and mitigate human error in the interpretation of medical images. Furthermore, the research offers a comparative assessment to current methodologies and establishes the superiority of the suggested approach, thus providing empirical substantiation for its efficacy. The primary contribution of this study lies in its potential to augment the early detection of lung cancer, expedite appropriate medical intervention, enhance patient outcomes, and contribute to the progress of medical image analysis methodologies. The significance of this study lies in several aspects:

- Improved lung cancer detection: By proposing a novel methodology that combines CNNs with an improved version of the Snake optimization algorithm, this study aims to enhance the accuracy and efficiency of lung cancer detection.
- Automation and efficiency: Manual interpretation of medical images is time-consuming and subject to human error. Automatic machine vision techniques, such as the one proposed in this study, can significantly streamline the lung cancer detection process.
- Novel use of the Snake optimization algorithm: The study introduces a modified version of the Snake optimization algorithm, specifically tailored for optimizing the design of CNNs used for lung cancer detection. By incorporating this improved variant of the algorithm into the CNN structure, the model's performance is further enhanced, demonstrating the potential of the Snake optimization algorithm in optimizing deep learning models for medical image analysis.
- Comparative evaluation and validation: To assess the effectiveness of the proposed methodology, the study evaluates its performance

against the widely used "IQ-OTH/NCCD-Lung Cancer Dataset" and compares it with other published methods in the literature.

- Potential clinical implications: The successful implementation of an optimized CNN model for lung cancer detection can have significant clinical implications. Accurate and efficient identification of lung cancer in CT images can aid healthcare professionals in making timely and informed decisions regarding treatment strategies.

In summary, this study's significance lies in its contribution to the field of lung cancer detection by proposing an improved methodology that combines CNNs with an optimized version of the Snake optimization algorithm. The findings showcase the potential of this approach in achieving accurate and efficient lung cancer detection, offering promising prospects for improved patient care and outcomes.

2. Dataset description

The performance of the offered procedure is examined in the current study using the "IQ-OTH/NCCD-Lung Cancer Dataset" which stands for Iraq Oncology-teaching Hospital or National Center Specialized for Cancer Diseases. In the fall of 2019, the IQ-OH/NCCD dataset is gathered over a three-month period from designated hospitals. This information includes computed tomography (CT) scans of lung cancer patients and healthy individuals at various phases of the disease. The dataset has been annotated by oncologists and radiologists as well. The IQ-OH/NCCD collection comprises 110 patients and includes 1190 CT pictures. The dataset has 3 types of benign, malignant, and healthy instances. 55 instances were classified as normal cases, 15 as benign, and 40 as malignant. The images are in DICOM format. All images were downloaded from the Kaggle website in "*.jpg" format [18]. From the IQ-OH/NCCD dataset, Fig. 1 shows some CT pictures of lung cancer and benign cases. Fig. 2.

These sample images serve to give an overview of the types of cases present in the dataset and provide a visual reference for the subsequent analysis and results discussed in the study.

3. Preprocessing

3.1. Image normalization

In the first stage, the input image brightness has been normalized between zero and one. For normalizing the images' brightness, the following formula is employed [19]:

$$I_{norm} = (I - I_{min}) \times \frac{I_{max}^{new} - I_{min}^{new}}{I_{max} - I_{min}} + I_{min}^{new} \quad (1)$$

where I designates the input image that is bounded between I_{min} and I_{max}, and I_N is the new normalized image that is bounded between I_{min}^{new} and I_{max}^{new}. Then, every picture in the dataset is scaled down to 250×250.

This resizing process ensures uniformity in terms of image dimensions, enabling easier comparison and analysis of the images during subsequent stages of the study. By normalizing the brightness and resizing the images, the dataset is prepared for further analysis, such as feature extraction or classification algorithms. These preprocessing steps contribute to the overall reliability and accuracy of the subsequent stages of the study, allowing for meaningful insights and conclusions to be drawn from the proposed Lung Cancer Dataset.

3.2. Median filtering

Image noise removal can be considered as either an image processing phase or a separate step. Image noise removal is a helpful tool to

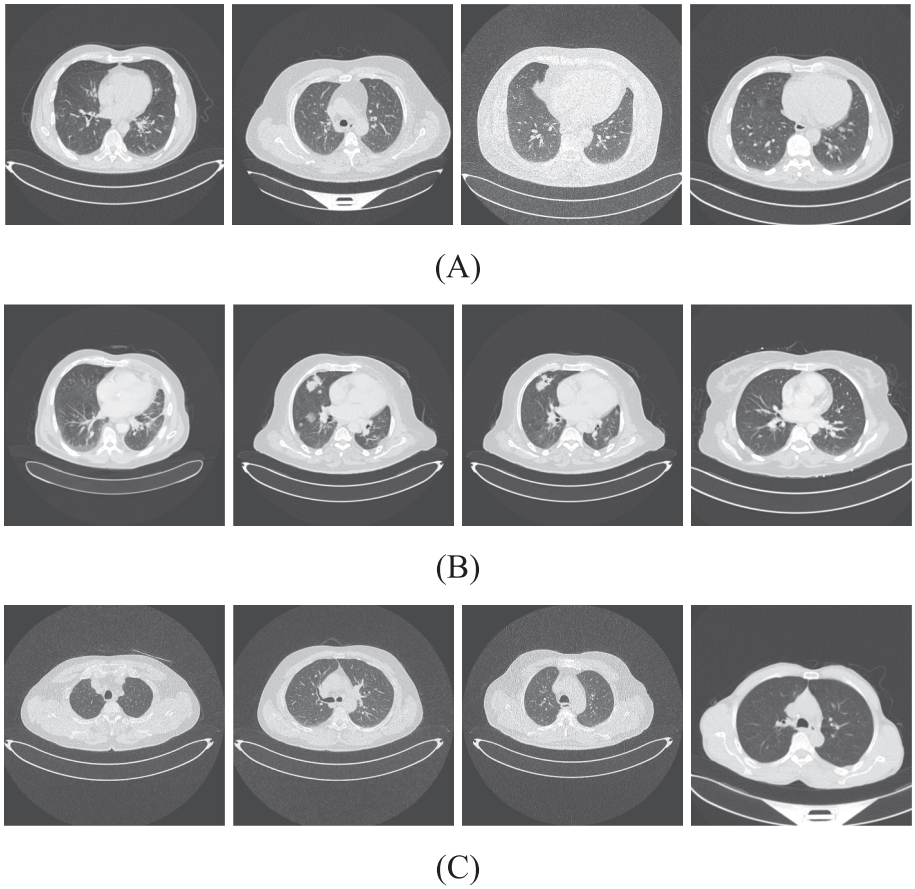

Fig. 1. Sample pictures of IQ-OTH/NCCD-Lung Cancer Dataset: (A) Malignant, (B) Benign, (C) Healthy cases.

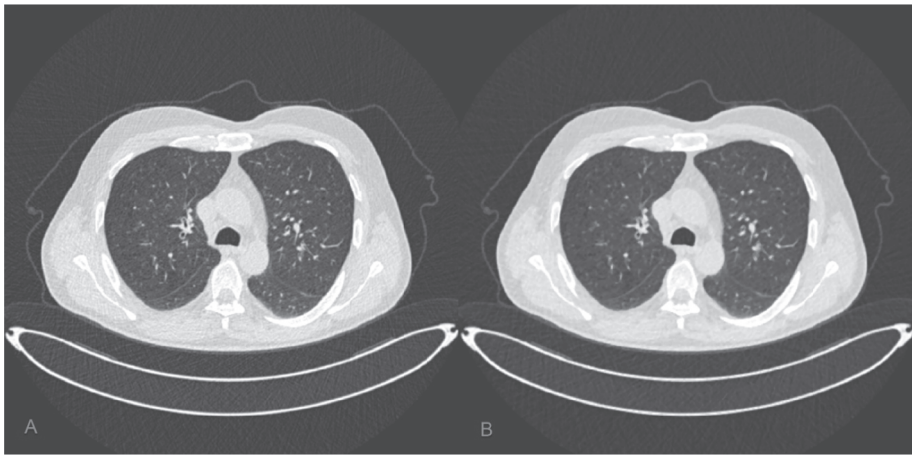

Fig. 2. A noise reduction sample by median filtering.

improve various image processing accuracy approaches, like classification [20]. Particularly in medical applications, it is crucial to preserve pertinent image data since improper noise reduction in diagnostic applications could cause problems with subsequent analysis, which could lead to incorrect final diagnoses by the experts [21]. As a result, noise reduction in medical pictures, especially in computed tomography (CT) imaging, which is often used in medicine, is one of the most important issues that has to be addressed.

A median filter has been used to reduce image noise. To eliminate the impacts of noise in the input pictures, the median filter specifies a popular non-linear filter [22]. The mask size should be proportionate to the original picture to provide appropriate filtering. We utilized a 3×3 window to digitally capture images and a MATLAB method to remove noise based on trial and error [23]. A pixel is substituted with the median amount of its entire surrounding pixels (the median filter), i.e.

$$y_{m,n} = median\left(x_{i,j}, (i,j) \in \theta\right) \tag{2}$$

Here, θ represents the user's neighborhood, centered in the (m,n) of the image. A noise reduction instance by median filtering is represented in Fig.

Noise is frequently encountered in the image acquisition process or as a result of diverse environmental factors. Random variations in pixel values can manifest as undesired distortions and lead to a decrease in the visibility of crucial details within the image. In order to mitigate the effects of noise, various filtering techniques are implemented, among which median filtering is a commonly utilized method. The application of median filtering involves the substitution of the value of each pixel in an image with the median value derived from the surrounding pixels. This technique is categorized as a non-linear filtering method. The aforementioned technique successfully mitigates the impact of abrupt fluctuations in intensity resulting from noise, while simultaneously retaining crucial features and boundaries within the image.

3.3. Contrast enhancement

Most recorded images have low image quality due to the limits of the cameras, making it often impossible to see the main characteristics of the items [24]. Typically, this flaw is referred to as gamma distortion. The majority of the time, traditional techniques like histogram equalization cannot overcome this problem. The gamma correction technique is an appropriate way to remove this sort of distortion from the collected devices [25]. This approach uses an adjustable parameter called Gamma (γ) to make an improvement in the image contrast quality on a histogram basis [26]. This technique uses a nonlinear filter to modify the brightness of the image based on the predetermined Gamma parameter. The general form transformed gamma correction (TGC) for the image under consideration is achieved by the following equation.

$$TGC = I_M \left(\frac{I_i}{I_M}\right)^{\gamma} \tag{3}$$

where, γ describes an adjustable parameter greater than zero, and I_i and I_M represent the image intensity, and its maximum intensity value, respectively.

the γ parameter affects the image pixel intensity, where,

If $\gamma = 1$, no modifications are made to the original image. On the other hand, if γ is lesser than one, the brightness is improved, and if γ is greater than one, the brightness is reduced, i.e., γ choosing directly influences the intensity of the image. Accordingly, Choosing the best amount for γ is of primary importance. Fig. 3 shows an example of image contrast enhancement by gamma correction.

The figure comprises two sub-figures, denoted A and B, which display the input image and the resulting image obtained after the application of gamma correction. Additionally, the histograms corresponding to each image are also presented. The application of gamma correction is a prevalent non-linear adjustment technique utilized to modify the contrast and brightness of images. The process entails the application of a power function to every individual pixel value within the image, leading to a modification of the distribution of pixel intensities. In sub-figure A, the input image is depicted before any form of correction or enhancement. The initial image may display inadequate contrast, wherein specific areas appear excessively dark or bright, thereby impeding the ability to perceive crucial details. The utilization of gamma correction can effectively mitigate this concern and enhance the perceptual fidelity of the image. The outcome depicted in sub-figure A demonstrates the impact of implementing gamma correction. By manipulating the gamma value, it is possible to augment the disparity in the contrast between distinct areas within the image, thereby accentuating subtle intricacies and ameliorating the overall perceptibility. This facilitates enhanced analysis and interpretation of the visual content in various applications, including medical imaging and computer vision. Figure B presents the histograms of both the input image and the resulting image. Histograms offer a visual depiction of the distribution of pixel intensities within an image. The observation of the impact of gamma correction on pixel values can be facilitated through the comparison of histograms. The process of gamma correction involves the redistribution of pixel values, which has the potential to expand the range of intensities and enhance the overall distribution.

3.4. Image data augmentation

A fundamental step in deep learning-based machine learning is data augmentation. The most intriguing and challenging element of deep

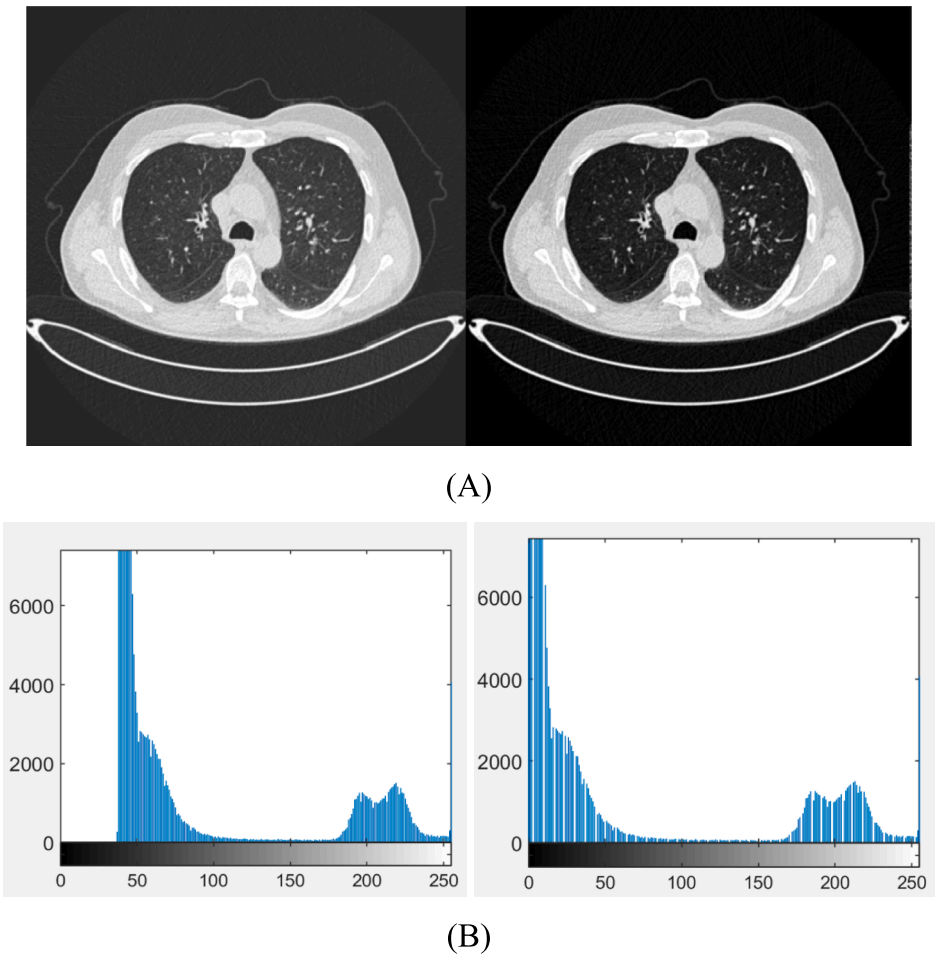

Fig. 3. Example of image contrast enhancement by gamma correction: (A) input image and result in the image, (B) their histograms.

neural networks is the issue of unequal class distribution. The term "Class Skew", which refers to the uneven distribution of samples across classes, implies unequal distribution of samples across classes. It's possible that the samples' quantity in one class and their numbers in another class are different, or that the samples in the two classes are very different. In datasets for two-folded classification, the distribution is unequal (e.g., here, we have lung cancer and healthy cases).

Each class's sample size should be about identical in order for the model to successfully complete the learning phase with no bias. On the other hand, the number of samples in the second class may be the same or less than the number of observations in the first class. In this instance, a class with more instances than a class with fewer examples results in the model learning more effectively. At last, we'll have a bias model that performs better in a class with more examples and generates predictions with more accuracy. All datasets suffer from the issue of unequal sample distribution across classes. Such datasets cannot be used to train any artificial intelligence technique. The SMOTE technique here is employed for data augmentation.

Since certain small occurrences are very simple to learn, the SdSmote procedure is a new data augmentation technique that has been popular. Cases that are challenging to understand must be picked since not all minority examples can be used to create a new synthetic instance [5,27–31]. Near the decision border, which is where these samples are frequently found, most algorithms search for false data. The goal of this technique is to select boundary samples from which to create fictitious samples. To do this, a variable called the degree of support is defined and generated utilizing the concept of sample distance.

The sample distance between the negative and positive class samples is determined by x_i and x_j according to the following equation, given that the negative and positive data sets are m and n, respectively.

$$S_j = \sum_{i=1}^{n} \sqrt{\|x_j - x_i\|^2}$$

$$S = \sum_{j=0}^{m} S_i \tag{4}$$

Then, the average distances can be obtained as follows:

$$\overline{S} = \frac{S}{n \times m} \tag{5}$$

4. Convolutional neural network (CNN)

4.1. CNNs

It is demonstrated that deep learning can manage a lot of data. In image processing, this technique has grown to be quite effective [32,33]. CNNs are a type of Deep NN that is very well-liked, and they are a unique kind of Neural Network (NN). The fact that deep learning models demand a lot of computational power and a lot of data for training is a key disadvantage [34]. However, one key disadvantage of deep learning models is that they require a large amount of computational power and a lot of data for training. The training process involves adjusting the parameters of the model in order to minimize the difference between the model's predictions and the actual values in the training data. This requires an enormous amount of computational resources, including specialized hardware such as graphics processing units (GPUs) or tensor processing units (TPUs).

In addition, deep learning models require a large amount of data in order to achieve high levels of accuracy and generalization. This is because these models often have a very large number of parameters, which need to be trained on a diverse set of examples in order to avoid overfitting and to ensure that the model can generalize to new, unseen data. The need for large amounts of data can be particularly challenging for medical applications, where data may be limited or difficult to obtain.

For a while, its usage was restricted to postal departments, but with the development of powerful hardware and an increase in machine processing power, it became widely accepted in many sectors, particularly machine vision [35]. The CNN is designed based on the visual cortex and has an architecture that resembles the connections between neurons in the brain. The design of CNNs is based on the idea that the visual cortex in the brain performs a similar process of feature extraction and hierarchical processing and that this process can be emulated using a set of learnable filters and nonlinear activation functions. By designing CNNs in this way, researchers have been able to achieve state-of-the-art performance on a wide range of image processing tasks, including object recognition, segmentation, and detection.

One may see a region because small groups of vision neurons work together to form linked networks in each portion of the brain. Convolutional neural network architecture comprises several kinds of layers, namely Conv (convolutional), POOL (pooling), and FC (fully connected) [36].

A fully convolutional network design is produced by combining these layers. Input, FC, Conv, POOL, and RELU layers can all be included in an architecture to accomplish this. The input layer contains the input image's raw pixel counts. So, an image will be present here. The Conv layer figures out how many neurons connected with particular regions at the input will produce. In the computation, points between each neuron's weight and the region to which it is connected are additionally multiplied (input activation mass).

Each neuron has an activation function assigned to it by the RELU layer, like maximum (0, x), which lowers the threshold to 0 and treats negative values as zero. As a result, the mass's size is unchanged from the previous phase. The POOL layer employs the technique of down sampling along the width and height. The input mass dimension has been reduced in this layer. Eventually, we obtain a score vector mostly over the activity of this layer. The class grade must be evaluated by the FC layer.

Like normal neural networks, each neuron in this network communicates with whole the neurons in the mass afore it.

Like so, the ConvNet transforms the primary image's raw pixel values into classes at the network's end. Be aware that certain layers have parameters while others do not. Conv/FC layers, in particular, are layers that execute conversions that depend on factors like weight and the bias of the neurons as well as activations in the input mass. In contrast, RELU/POOL layers only apply one fixed function. The convolution network's class scores will match the labels of each picture in the training set since the parameters in the Conv/FC layer are trained using the descent gradient method.

Different settings are provided for the proper construction of convolutional neural networks. Conv neural networks have two layers and several hyperparameters. For instance, in a CNN, the stride of kernels, and sizes; the number of kernels, activation function, in the POOL layer, kernel size related to max-pooling, learning rate; in the dense layer; quantity of convolutions, pooling, and dense layers, and the layer size.

4.2. Objective function

The choice of a CNN's hyperparameters can be considered an optimization issue. Finding the optimum hyperparameters as decision variables to provide optimal results on the objective function will therefore be the main focus. In this research, the cost function is the model accuracy. Therefore, the main objective is to employ an optimization technique to improve accuracy, specifically:

$$\max_{\overrightarrow{H_p} \in R^i} CNN\left(\overrightarrow{H_p}, \vec{W}, Td_i\right) \tag{6}$$

where, Td_i represents training data, $\overrightarrow{H_p}$ represents the hyperparameter vector in the dimension i, CNN specifies the weight vector, and $i^{max}(> i)$ establishes a predefined parameter that compromises the accuracy of the algorithm with the complexity of the algorithm.

Here, the high value of the term will show the high complexity of the network, and vice versa. The suggested approach uses a pipeline methodology that includes picture preparation, data analysis, and the use of an ideal convolutional network built for lung cancer diagnosis. The next section will go into great detail on the methodology.

4.3. Optimal arrangement of the CNN

By considering the explanations before, each layer of the convolutional neural network has different hyperparameters that should be properly selected to provide better efficiency. Normally, these hyperparameters are achieved by experimental establishments. In this study, to provide an optimal network design, we consider a modified metaheuristic algorithm, called the improved Snake Optimization algorithm. In this study, three layers are considered for the activation function, the convolution layer, the pooling layer, and the dropout layer. This arrangement is then completed by integrating two dense layers and one flatten layer.

Simple features are chosen in the first layer and advanced features are created in later layers, according to the kernel number of layers, which sets the designated characteristics for the subsequent layers. The pooling size controls a crucial hyperparameter in POOL layers. The input features are down-sampled and pushed to the next layer based on this hyperparameter. The network is significantly impacted by keeping a balance for the size of the POOL layers, therefore a larger percentage for this feature results in disdain for minute details. POOL layers are typically used to downsample the feature maps produced by the convolutional layers, in order to reduce the computational cost and improve the model's robustness to small variations in the input image. in general, Overall, keeping a balance for the size of the pooling layers is an important consideration when designing a CNN, as it can have a significant impact on the model's performance and generalization ability. By carefully tuning the pooling parameters and balancing spatial resolution with feature extraction, researchers can develop CNNs that are optimized for specific image processing tasks.

The size distribution of the POOL layer in this research is between 3 and 5. The rate of dropout layers is the main determining factor and improper value selection results in overfitting. The dropout rate in this study is predicted to range between 20% and 60%. To reduce underfitting and overfitting by the Conv layer, as well as the production of repeating features, the number of Conv layer and POOL layer is restricted in the range [3,9]. Firstly, the number of repeating features and layers in a CNN can have a significant impact on the model's performance and training time. Too few layers or features may result in a model that is too simple and unable to capture the complex patterns in the data, while too many layers or features may result in a model that is too complex and prone to overfitting. Additionally, adding more layers or features can significantly increase the computational cost and training time, which can be prohibitive for resource-constrained applications. Secondly, the optimal number of layers and features may vary depending on the specific task and dataset. For example, a simple image classification task may require fewer layers and features than a more complex task such as object detection or semantic segmentation. Similarly, the optimal number of layers and features may depend on the size and complexity of the input images, as well as the amount of available training data. Finally, the number of layers and features in a CNN is often limited by practical considerations, such as the availability of

computational resources and memory constraints. For example, a model with a very large number of layers or features may not be able to fit into the memory of a standard GPU or CPU, which can limit its practical utility.

After determining the workable range, a large number of experiments are essential to determine the optimum network design. However, we want to select the best CNN parameter value utilizing the suggested improved Snake Optimization algorithm that has been provided.

In the current study, the kernel number (N_k), rate of dropout (R_d), and kernel size (S_k) from the Conv layer, together with the kernel size (P_k) in the POOL layer, are selected as the network's optimum parameters using the proposed improved Snake Optimization algorithm. Accordingly, the technique includes a d-dimensional vector and the matching set of decision variables, as shown in the following example:

$$d = 2N_{conv} + N_{pool} + N_d \tag{7}$$

where N_d, N_{POOL}, and N_{conv} represent the number of dropout rates, the POOL layer, and the Conv layer. The definition of the j^{th} the parameter is as follows:

$$\overrightarrow{HP_j} = \left[P_j^1, P_j^2, \cdots, P_j^k\right] \tag{8}$$

Here, by considering 12 decision variables including the hyperparameters of the Conv layer, POOL layer, and dropout (Drop) layer, i.e.,

$$[Conv_{N_k}^1, Conv_{S_k}^1, Pool_{P_k}^1, Drop_{R_d}^1, Conv_{N_k}^2, Conv_{S_k}^2, Pool_{P_k}^2, Drop_{R_d}^2, Conv_{N_k}^3, Conv_{S_k}^3, Pool_{P_k}^3, Drop_{R_d}^3] \tag{9}$$

The set of n solutions will be randomly obtained as follows:

$$S_n = \left[\overrightarrow{HP_1}, \overrightarrow{HP_2}, \cdots, \overrightarrow{HP_n}\right] \tag{10}$$

5. The improved Snake optimization algorithm (iSOA)

5.1. Original Snake optimization (SO)

In this part, inspiration and mathematical expression related to snake optimization are described.

A. The behavior of snake pairing.

Snakes mate at the end of spring and the beginning of summer. They mate in cold places, that is, where the temperature is low. Likewise, one of the other influential factors in the mating of snakes is food availability. When food is accessible and the temperature is low, male snakes compete and combat for the attention of female snakes. The female decides to mate and in case of mating, she begins laying eggs in a lair and leaves it after the eggs come out.

B. Source of motivation.

The pairing behavior of snakes is a motivation for snake optimization (SO). If the mating conditions mentioned in the previous section are not suitable, the snakes will just explore for food or eat the existing food. The search strategy, considering the different behavior of snakes in different conditions, includes two stages exploration and exploitation. In the exploration phase, environmental conditions are examined, i.e. conditions where there is no food and cold place, so snakes just look for food in their surround.

In the exploitation phase, transitional steps are used for a more effective global search. In conditions where the temperature is high and food is accessible, the focus of the snake is on eating existing food. Mating starts when the place is cold and food is accessible. The pairing process includes two stages fighting and mating. In the fighting case, the fight between males is to obtain the finest pair, and any female wants to choose the finest pair as well. When it comes to the pairing case, the amount of food that is available determines the mating between snakes. If the pairing approach happens throughout the search area a possibility exists that the female is likely to lay eggs and create new snakes.

C. Algorithm and mathematical model.

The details of the offered algorithm are scrutinized in the following:

- *Initialization*

At the beginning of the process, a random population with a uniform distribution is generated. The equation given below describes the attainment of the initial population.

$$Z_i = Z_{min} + r \times (Z_{max} - Z_{min}) \tag{11}$$

Here is the location of i^{th} the individual is indicated by Z_i, the higher and lower ranges of the problem are represented by Z_{max} and Z_{min}, r is a random amount between (0,1).

- *Splitting the population into two identical crowds of males and females*

Each the number of women and men is considered 50%. The swarm is split into two sets: a male group and a female group. The following equations are employed to split the population:

$$N_m \approx N/2 \tag{12}$$

$$N_f = N - N_m \tag{13}$$

where N defines the number of the population, the male and female individual numbers are indicated by N_m and N_f.

- *Assessing each of the groups and determining the amount of food and temperature*
- The finest man ($f_{b,m}$) in the men's group and the finest woman ($f_{b,f}$) in the women's group are determined. Also, the location of the food (f_{food}) is obtained.
- The following equation defines the Temperature Temp in this algorithm

$$Temp = \exp(-\frac{t}{T}) \tag{14}$$

where t states the present iteration and T states the max number of iterations.

- Determining the quantity of food (Q) The quantity of food can be acquired utilizing the below equation:

$$Q = c_1 * \exp(\frac{t-T}{T}) \tag{15}$$

Here c_1 indicates a fixed number equal to 0.5.

- *Exploration stage (lack of food)*

If Q is less than the threshold which is equal to $\frac{25}{100}$, the snakes look for nutrition by choosing any haphazard place and updating their location. The simulation of the exploration stage is as below:

$$Z_{i,m}(t+1) = Z_{rand,m} \pm c_2 \times A_m \times ((Z_{max} - Z_{min}) \times rand + Z_{min}) \tag{16}$$

where $Z_{i,m}$ relates to i^{th} male location, $Z_{rand,m}$ relates to the location of an

arbitrary male, *rand* indicates a random amount in the interval 0,1, and the male capability to discover the food is represented by A_m which is computed as below:

$$A_m = \exp(\frac{-f_{rand,m}}{f_{i,m}}) \tag{17}$$

In which $f_{rand,m}$ indicates the fitness of $Z_{rand,m}$, and $f_{i,m}$ represents the fitness of i^{th} individual male set and c_2 is a fixed number equal to 0.05.

$$Z_{i,f} = Z_{rand,f}(t+1) \pm c_2 \times A_f \times ((Z_{max} - Z_{min}) \times rand + Z_{min}) \tag{18}$$

Where $Z_{i,f}$ relates to i^{th} female location, $Z_{rand,f}$ relates to the location of an arbitrary female, *rand* indicates a random amount in the interval 0,1, and the female capability to discover the food is represented by A_f which is computed as below:

$$A_f = \exp(\frac{-f_{rand,f}}{f_{i,f}}) \tag{19}$$

In which $f_{rand,f}$ indicates the fitness of $Z_{rand,f}$, and $f_{i,f}$ represents the fitness of i^{th} individual female set.

- *Exploitation stage (presence of food)*

If Q is more than 0.25; If the temperature is more than the threshold which is equal to 0.6 (hot place), the movement of snakes is only toward food.

$$Z_{i,j}(t+1) = Z_{food} \pm c_3 \times Temp \times rand \times (Z_{food} - Z_{i,j}(t)) \tag{20}$$

Here the location of the individual is indicated by $Z_{i,j}$, the location of the finest candidates is defined by Z_{food}, and c_3 indicates a fixed amount equal to 2.

If the temperature is less than 0.6 (cold place), one of the cases of fighting or mating occurs.

Mode of Fight

$$Z_{i,m}(t+1) = Z_{i,m}(t) + c_3 \times FM \times rand \times (Q \times Z_{b,f} - Z_{i,m}(t)) \tag{21}$$

where $Z_{i,m}$ states the i^{th} male location, $Z_{b,f}$ states the location of the finest individual in the female set, and *FM* indicates the fighting capability of a male individual.

$$Z_{i,f}(t+1) = Z_{i,f}(t+1) + c_3 \times FF \times rand \times (Q \times Z_{b,m} - Z_{i,F}(t+1)) \tag{22}$$

where $Z_{i,f}$ states the i^{th} male location, $Z_{b,m}$ states the location of the finest individual in the male set, and *FF* indicates the fighting capability of the female individual.

The computation of *FF* and *MF* are as below:

$$FF = \exp(\frac{-f_{b,m}}{f_i}) \tag{23}$$

$$FM = \exp(\frac{-f_{b,f}}{f_i}) \tag{24}$$

where $f_{b,f}$ indicates the fitness of the finest individual of the female set, $f_{b,m}$ indicates the finest individual of male set's fitness, and f_i defines individual fitness.

Mode of mating:

$$Z_{i,m}(t+1) = Z_{i,m}(t) + c_3 \times M_m \times rand \times (Q \times Z_{i,f}(t) - Z_{i,m}(t)) \tag{25}$$

$$Z_{i,f}(t+1) = Z_{i,f}(t) + c_3 \times M_f \times rand \times (Q \times Z_{i,m}(t) - Z_{i,f}(t)) \tag{26}$$

Here is the location of i^{th} individual in the female set is indicated by $Z_{i,f}$, and the location of i^{th} individual in the male set is indicated by $Z_{i,m}$, the capability of mating for males and females is defined by M_m and M_f as below:

$$M_m = \exp(\frac{-f_{i,f}}{f_{i,m}}) \tag{27}$$

$$M_f = \exp(\frac{-f_{i,m}}{f_{i,f}}) \tag{28}$$

If eggs hatch, choose and replace the worst male and Female:

$$Z_{w,m} = Z_{min} + rand \times (Z_{max} - Z_{min}) \tag{29}$$

$$Z_{w,f} = Z_{min} + rand \times (Z_{max} - Z_{min}) \tag{30}$$

where $Z_{w,m}$ and $Z_{w,f}$ indicate the worst agent in the male and female sets. The diversity factor $\pm$ can cause to increase or decrease in locations' solution, so it creates many opportunities to alter the direction of the factors, and as a result, the provided solution space is well-searched in all directions. This parameter is created at random for attaining the randomization characteristic which is necessary for all *meta*-heuristic algorithms.

- *Checking the end conditions*

The flow will persist for a numeral of iterations from phase 2, if the criterion is met the operation will be ended.

5.2. The improved Snake optimization (iSO) algorithm

As mentioned before, the standard Snake optimizer is anew offered metaheuristic algorithm, being proposed for solving different kinds of optimization problems [37,38]. Although the analyses in the main paper of this algorithm show efficient results for different problems, it needs global search proficiency early in the algorithmic process and global convergence to provide more efficient results. The present study introduces two modifications to the Snake optimizer to provide far more effective outcomes for the original algorithm.

The first modification is to utilize a chaos mechanism in the Initialization stage. However, the original Snake Optimization algorithm in the initialization stage, provides a random distribution to make the solution candidates, by rising the solution space size, providing a good distribution solution for the problem gets complicated; this has a significant effect on the solver search efficiency. To modify the algorithm in this term of view, the start positions have been made based on the pseudo-random chaotic sequences. This method not only increases the processing speed but can also improve the search distribution based on the chaotic sequences. Here, we used the following function for this purpose[39]:

$$Z_{i,j}(t+1) = \alpha \times Z_{i,j}(t) \times \left(1 - Z_{i,j}(t)\right) \tag{31}$$

where, α, bifurcation coefficient, specifies a determined value limited between 3.57 and 4, and $Z_{i,j}(t)$ describes a chaotic parameter that is spread between 0 and 1, where, $Z_{i,j}(t) \notin [0,\ 0.25,\ 0.5,\ 0.75,\ 1]$ [39].

The second modification for the proposed method is to use the sigmoid-based acceleration coefficient. This technique can assist the algorithm to make a great balance between the algorithm convergence velocity and its better global solution searching.

The textual version of the sigmoid-based acceleration coefficients applied to R yields:

$$r_k = \frac{1}{1 + \exp(-\theta t)} + 2\left(r_f - r_i\right)(t-1)^2 \tag{32}$$

where, θ signifies the adjusting parameter in Eq. (11) that is improved based on the sigmoid acceleration constants (where, $\theta = 0.002$), $r_i = 0.2$ and $R_f = 1$ represents two constants, τ characterizes the present iteration times k to the maximum iteration times M.

Whereas $t = 0$, the value of R starts to reduce nonlinearly from 2,

Table 1
Specifics about the benchmark functions utilized in this research.

Equation	Function	Range
$F_1 = \sum_{i=1}^{n} x_i^2$	Sphere	[-100,100]
$F_2 = \sum_{i=1}^{n} \lvert x_i \rvert + \prod_{i=1}^{n} \lvert x_i \rvert$	Schwefel 2.22	[-10,10]
$F_3 = \sum_{i=1}^{n} \left(\sum_{j=1}^{i} x_j \right)^2$	Schwefel 1.2	[-100,100]
$F_4 = \lfloor \lvert x_i \rvert \quad \mathrm{n} \geq i, i \geq 1 \rfloor$	Schwefel 2.21	[-100,100]
$F_5 = \sum_{i=1}^{n-1} \left\lvert (x_i - 1)^2 + 10^2 (x_{i+1} - x_i^2)^2 \right\rvert$	Rosenbrock	[-31,31]
$F_6 = 20 + \mathrm{e} - 20e^{-\frac{1}{5}(\sqrt{\sum_{i=1}^{n} x_i^2})} - e^{\frac{1}{n}(\sqrt{\sum_{i=1}^{n} coscos(2\pi x_i)})}$	Ackley	[–32,32]
$F_7 = \frac{1}{4000} \sum_{i=1}^{n} x_i^2 - \prod_{i=1}^{n} \mathrm{coscos}\left(x_i \times i^{-\frac{1}{2}} \right)$	Griewank	[-600,600]
$F_8 = \sum_{i=1}^{n} \left\lvert x_i \mathrm{sinsin}(x_i) + \frac{x_i}{10} \right\rvert$	Alphine 1	[-10,10]
$F_9 = \prod_{i=1}^{n} \left\lvert \mathrm{sinsin}(x_i) x_i^{\frac{1}{2}} \right\rvert$	Alphine 2	[-10,10]
$F_{10} = \sum_{i=1}^{n} x_i x_{i-1} + \sum_{i=1}^{n} (x_i - 1)(x_i - 1)$	Trid	[-100,100]

causing the starting vectors to divide into the search space. After regulating t to 1, the R value is decreased to 0.5. This increases the Snake Optimization algorithm to reach the supreme solution.

5.3. Validation of the iSO algorithm

This section examines how well the suggested improved Snake Optimization (iSO) algorithm performs when it comes to tackling optimization problems. Ten objective functions of various unimodal and multimodal functions, containing 5 unimodal and multimodal functions (F1-F5) and (F6-F10), are solved for this purpose using the suggested iSO algorithm. Table 1 contains specifics about the benchmark functions utilized in this research.

Additionally, a comparison is conducted among the results of the proposed iSO algorithm, the original SO algorithm, and three other optimization techniques, namely Squirrel search algorithm (SSA) [40], Supply-Demand-Based Optimization (SDO) [41], and Biogeography-Based Optimizer (BBO) [42]. Table 2 illustrates the amounts of the control variables utilized by these algorithms.

35 different implementations, each having 250 iterations, of the competing methods and the proposed iSO algorithm have been carried out on the objective functions for the evaluation of the optimization algorithms' performance. Two criteria are used to evaluate the simulation results: the best solutions' standard deviation, average, and best solutions' average (avg) (std). Eqs. (33) and (34) are used to calculate two average and std criteria:

$$AVG = \frac{1}{N} \sum_{j=1}^{N} z_j \tag{33}$$

Table 2
Values of the control parameters used by these algorithms.

Algorithm	Parameter	Value
Squirrel search algorithm (SSA) [40]	N_{fs}	5
	G_c	2.1
	P_{dp}	0.2
Supply-Demand-Based Optimization (SDO) [41]	MaxIteration	250
	MarketSize	35
	FunIndex	1
Biogeography-Based Optimizer (BBO) [42]	Probability of habitat alteration	1
	probability Immigrating per gene	0.5
	Size of Step for a mathematical combination of possibilities	1
	Max emigrating and immigrating (E) and (I)	1
	Probability of mutation	0.04

Table 3
The optimiziation results of the F1 to F10 functions.

Benchmark		iSO	SO [43]	SSA [40]	SDO [41]	BBO [42]
f1	AVG	0.00	3.15	4.51	4.62	3.28
	STD	0.00	2.42	4.36	4.42	3.19
f2	AVG	1.13	2.62	3.42	3.47	3.17
	STD	0.93	2.16	3.11	3.28	3.03
f3	AVG	0.00	3.25e-9	3.31e-8	4.06e-8	2.26e-9
	STD	0.00	0.00	3.43e-8	4.25e-8	2.21e-9
f4	AVG	0.00	0.00	4.62e-8	5.83e-7	4.83e-8
	STD	0.00	0.00	4.94e-8	6.14e-7	5.01e-8
F5	AVG	0.00	1.36	2.62	2.94	1.26
	STD	0.00	1.23	2.39	2.48	1.15
F6	AVG	0.03	3.12	3.51	3.73	3.21
	STD	0.00	2.77	3.24	3.66	3.16
F7	AVG	0.00	3.83	4.15	4.24	3.67
	STD	0.01	3.53	3.76	4.19	3.37
F8	AVG	0.00	0.69	1.24	1.66	0.94
	STD	0.05	0.51	1.16	1.58	0.68
F9	AVG	0.001	0.25	0.63	0.55	0.34
	STD	0.00	0.11	0.52	0.38	0.13
F10	AVG	0.02	0.84	1.15	1.43	1.12
	STD	0.00	0.62	1.08	1.11	1.04

$$STD = \sqrt{\frac{1}{N} \sum_{j=1}^{N} \left(z_j - AVG \right)^2} \tag{34}$$

In the above equation, N represents the independent runs' quantity and z_j describes the best solution candidate achieved in the j^{th} run. The optimization outcomes of the F1 to F10 functions are illustrated in Table 3.

For function F1, the AVG results show that iSO achieves an optimal value of 0.00, while the other algorithms, including SO, SSA, SDO, and BBO, achieve higher AVG values ranging from 3.15 to 4.62. Function F2 again demonstrates that iSO has the lowest AVG value of 1.13, indicating a better optimization outcome compared to the other algorithms, which have AVG values ranging from 2.62 to 3.47. The optimization results for function F3 are close to zero for all algorithms, indicating successful convergence to the global optimum. However, iSO achieves a slightly better AVG value of 0.00 compared to the other algorithms. Function F4 follows a similar trend, with iSO achieving an AVG value of 0.00, while the other algorithms have higher AVG values ranging from 0.00 to 5.83e-7. Moving on to function F5, iSO once again outperforms the other algorithms with an AVG value of 0.00, while the AVG values for the other algorithms range from 1.26 to 2.94. For function, F6, iSO achieves an AVG value of 0.03, whereas the other algorithms achieve AVG values ranging from 3.12 to 3.73. Function F7 shows that iSO achieves an AVG value of 0.00, whereas the other algorithms achieve AVG values ranging from 3.83 to 4.24. Similarly, for function, F8, iSO achieves an AVG value of 0.00, whereas the other algorithms achieve AVG values ranging from 0.69 to 1.66. Function F9 demonstrates that iSO achieves an AVG value of 0.001, while the other algorithms achieve AVG values ranging from 0.25 to 0.63. Lastly, for function, F10, iSO achieves an AVG value of 0.02, while the other algorithms achieve AVG values ranging from 0.84 to 1.43.

As can be seen from the explanations before and Table 3, the unimodal type describes the goal functions of F1 through F6. On these functions, the suggested iSO method and four challenging algorithms are used. The outcomes of improving the F1 through F6 functions are displayed in Table 3. The global optimum of this function, which is zero, is reached by the suggested algorithm in the F1, F3, F4, and F5 optimization, according to this Table. According to the comparison of the efficacy of optimization algorithms, the iSO has provided results that are much more competitive and nearer to the global optimal than the competing algorithms. Five objective functions, numbered F6 to F10, have been chosen to compare the proposed iSO algorithm against four challenging algorithms in terms of optimizing multi-modal functions. On these goal functions, Table 3 also displays the outcomes of the

application of the iSO algorithm and four rival methods. With convergence to zero for F7–F10, the suggested iSO algorithm displays the global optimum. The suggested technique offers quasi-optimal solutions for additional F6 and is the first best optimizer in this regard. The suggested iSO method is competitive with four other comparable algorithms, according to analysis of the simulation data, and has a respectable capacity to tackle this sort of optimization issue. Finally, the lower standard deviation values across the board demonstrate the proposed method's improved consistency in solving optimization issues over several separate runs.

6. Simulation results

6.1. Execution details

A metaheuristic algorithm's results might vary with each run since they are stochastic. We thus conducted each test 25 times. Numerous methods, in addition to the proposed roved Snake Optimization (iSO) algorithm, can be used for the comparisons made in the preceding section [44]. For a fair comparison, each algorithm underwent a maximum of 250 iterations across 25 runs (6250 function calculations).

According to the high computing performance processing system, which comprises numerous computing clusters and their integration results in centralized task management, simulations have been performed in the 64-bit version of the Matlab R2018b programming environment [45]. Hardware has the following specifications: NVIDIA GeForce GTX 1080 Ti GPU card with an Intel Xeon CPU with 128 GB of RAM.

6.2. Authentication indicators

Six assessment metrics, including Jaccard Index (JI), specificity (Sp), precision (Pr), accuracy (Acc), F1-score, and sensitivity (Sen) have been used to validate the suggested technique (F-S). The mathematical formulation of the indicators is graphically shown in Fig. 4.

In Fig. 4, FN and TN demonstrate False Negative and True Negative. Also, TP and FP signify the True Positive and False Positive.

6.3. Results

In this section, two different authentications have been implemented. In the first stage, the model's effectiveness has been validated before and after preprocessing. In the second stage, a comparison is conducted among the outcomes of the model with preprocessing and some other published methods comprising KNN (k-Nearest neighbors) [46], integrated contrast/features-based method (CFM) [47], weakly supervised deep learning (WSDL) [48], Co-learning feature fusion maps (CLFM) [49], and DFD-Net [50]. 75% of the input images are trained to the network and 25% of those are employed as the test.

Table 4
Modeling outcomes of the scheme classification with and without preprocessing stage.

Method	Acc	Se	Sp	Pr	F-S	JI	Error
Method with preprocessing	96.58	95.38	94.08	84.16	91.53	89.44	3.42
Method without preprocessing	89.67	92.46	92.26	86.29	85.62	94.94	10.33

To indicate the effectiveness of using the preprocessing stage on the proposed method, the method is first compared with its results when the preprocessing stage has not been applied. The simulation outcomes of the technique classification with and without preprocessing stage are illustrated in Table 4.

As can be illustrated in Table 4, the method with preprocessing outperformed the method without preprocessing in all six assessment metrics, as well as in the overall accuracy. The difference in accuracy between the two methods was 6.91%, which is a significant improvement. The method with preprocessing also achieved higher sensitivity, specificity, precision, and F1-score, indicating that it was better able to correctly classify both positive and negative cases. Specifically, the method with preprocessing achieved a sensitivity of 95.38%, compared to 92.46% for the method without preprocessing. It also achieved a specificity of 94.08%, compared to 92.26% for the method without preprocessing. The Jaccard Index, which measures the similarity between the predicted and actual classes, was also higher for the method with preprocessing, indicating that it was better able to accurately capture the true positive and true negative cases. The error rate was also lower for the method with preprocessing, indicating that it made fewer mistakes in classification.

The test and training figures of the proposed method without and with preprocessing stage are demonstrated in Fig. 5.

Regarding Fig. 5, which shows the performance of the proposed methodology with and without the preprocessing stage, the results indicate that the use of preprocessing can significantly improve the accuracy of the system, as observed in both the training and test stages. Specifically, as shown in the figure, the accuracy of the system with preprocessing is consistently higher than the accuracy of the system without preprocessing, across both the training and test stages. This suggests that the preprocessing stage can effectively enhance the input data and extract more informative features, which in turn leads to more accurate and reliable classification results. Table 4 indicates some details about this analysis.

In the next step, to indicate the suggested procedure's effectiveness, a comparison is done between its results and other aforementioned

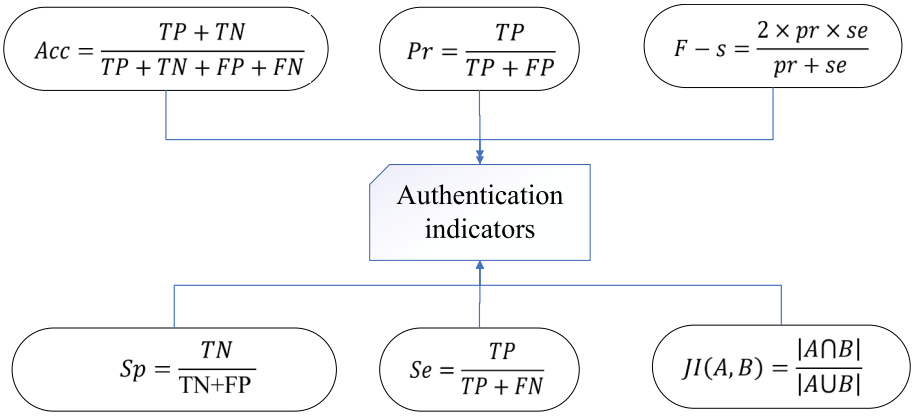

Fig. 4. Graphical definition of the authentication indicators.

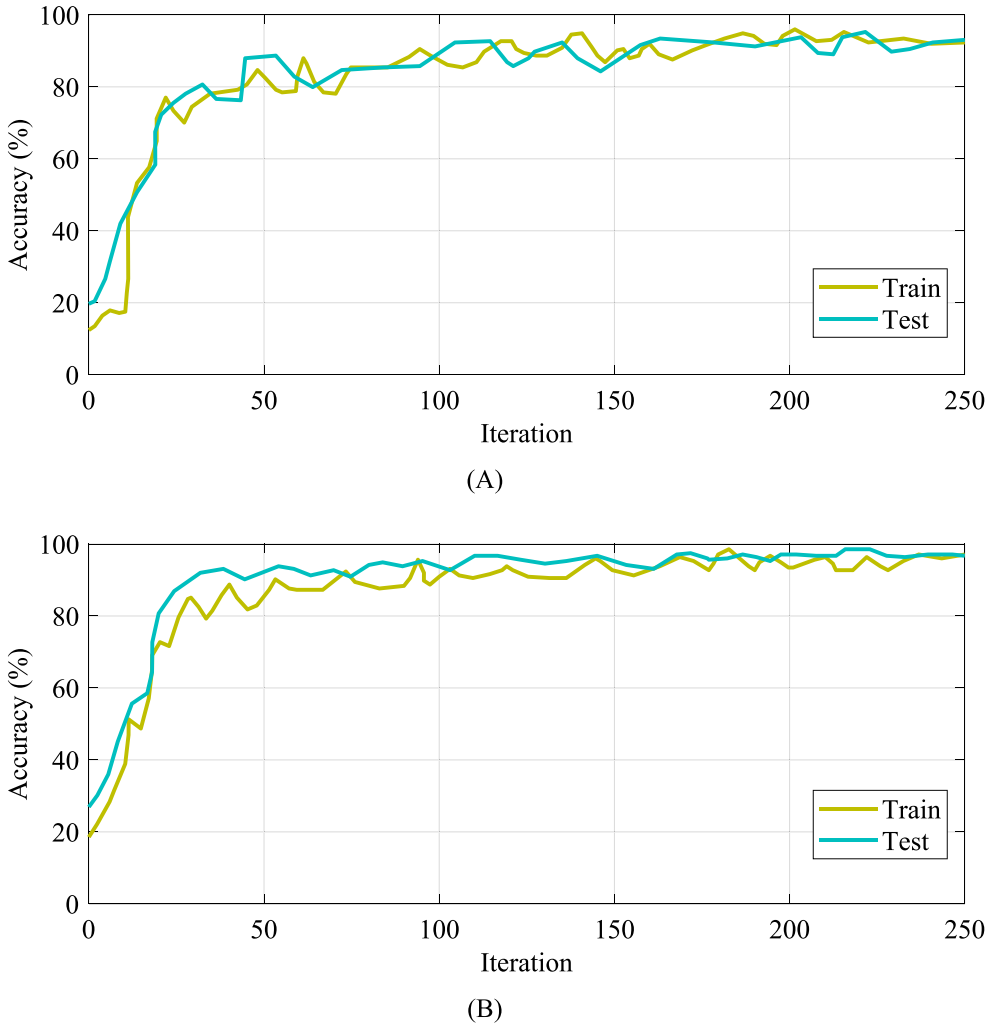

Fig. 5. Test and training profile of the offered method (A) without and (B) with preprocessing stage.

Table 5
Comparison results of diagnosis systema with other studied techniques.

Method	Acc	Se	Sp	Pr	F-S	JI	Error
Proposed method	96.58	95.38	94.08	84.16	91.53	89.44	3.42
KNN [46]	85.25	85.32	83.32	71.09	82.56	78.46	14.75
CFM [47]	87.24	87.24	86.65	75.94	84.19	81.19	12.76
WSDL [48]	89.26	89.16	88.46	78.26	86.37	83.61	10.74
CLFM [49]	92.46	91.08	90.39	81.39	88.34	85.37	7.54
DFD-Net [50]	94.52	93.65	92.46	83.50	89.90	87.49	5.48

techniques. Table 5 depicts the outcomes of this comparison.

About Table 5, the recommended method with 94.52% accuracy, which provides only a 3.42% error rate, provides the highest confirmation with the real values. Also, the 94.08% specificity of the proposed method which is the highest value among the other studied methods, shows the method's higher rate of true negative that describes its ability to correct non-tumor pixels diagnosis. With 95.38% sensitivity in the offered technique, its far greater ability in diagnosing the unaffected positive rate, which is its suitable diagnosis of similar pixels, is verified. 84.16% precision by the proposed method indicates the advanced similarity of the diagnosed images, though the 89.44% Jaccard Index of the method proves its higher ability in diagnosing during similarity.

7. Conclusions

The unrestrained growth of cells in lung tissues is the main thing that characterizes Lung cancer. This cell growth could disperse and reach surrounding tissues or other organs in a process called metastasis providing that the disease is not treated. The major kinds of this disease are SCLC (small cell lung cancer), also addressed by squamous cell carcinoma. Primary root cancer is by far the most prevailing cancer leading to death in both males and females. This current study developed a novel lung cancer diagnosis technique for detecting lung cancer in CT images. This strategy is an ideal solution for cancer diagnosis using convolutional neural networks (CNNs). According to the current study, after preprocessing the lung cancer photos, they were inserted into the best CNN. A new enhanced Snake Optimization technique was devised and used to the CNN's hyperparameters to give optimal CNN configuration. The suggested model was then evaluated using the IQ-OTH/NCCD-Lung Cancer Dataset. On numerous assessment metrics, the technique was verified against k-Nearest neighbors (KNN), integrated contrast/features-based method (CFM), weakly supervised deep learning (WSDL), Co-learning feature fusion maps (CLFM), and DFD-Net. The results endorsed that the suggested technique outperforms the other ones.

CRediT authorship contribution statement

Chaohua Yan: Conceptualization, Data curation, Writing – original draft, Writing – review & editing. **Navid Razmjooy:** Conceptualization, Data curation, Writing – original draft, Writing – review & editing.

Declaration of Competing Interest

The authors declare that they have no known competing financial interests or personal relationships that could have appeared to influence the work reported in this paper.

Data availability

No data was used for the research described in the article.

Acknowledgements

Henan Provincial Department of Science and Technology Provincial Key Research and Development and Promotion Project, Project Number: 222102320375, Project Title: Research on Key Technologies for Plant Image Recognition in the Danjiang Basin based on Multi-scale Convolutional Neural Network.

Nanyang Science and Technology Tackling Key Problems Project, Project Number: KJGG023, Project Title: Research on Rapid Retrieval Technology for Distributed Medical Image Data based on Cloud Platform.

References

[1] G. Aghajani, N. Ghadimi, Multi-objective energy management in a micro-grid, Energy Rep. 4 (2018) 218–225.
[2] *Key Statistics for Lung Cancer*, A.c. society, Editor. 2022: USA.
[3] Z. Ren, Y. Zhang, S. Wang, A hybrid framework for lung cancer classification, Electronics 11 (10) (2022) 1614.
[4] Z. Guo, et al., Novel computer-aided lung cancer detection based on convolutional neural network-based and feature-based classifiers using metaheuristics, Int. J. Imaging Syst. Technol. (2021).
[5] Z. Xu, et al., Computer-aided diagnosis of skin cancer based on soft computing techniques, Open Med. 15 (1) (2020) 860–871.
[6] fish 0,punct]">Q. Tian, et al., A New optimized sequential method for lung tumor diagnosis based on deep learning and converged search and rescue algorithm, Biomed. Signal Process. Control 68 (2021), 102761.
[7] N. Razmjooy, F.R. Sheykhahmad, N. Ghadimi, A hybrid neural network–world cup optimization algorithm for melanoma detection, Open Medicine 13 (1) (2018) 9–16.
[8] Y. Xu, Y. Wang, N. Razmjooy, Lung cancer diagnosis in CT images based on Alexnet optimized by modified Bowerbird optimization algorithm, Biomed. Signal Process. Control 77 (2022), 103791.
[9] N. Razmjooy, M. Ramezani, N. Ghadimi, Imperialist competitive algorithm-based optimization of neuro-fuzzy system parameters for automatic red-eye removal, Int. J. Fuzzy Syst. 19 (4) (2017) 1144–1156.
[10] X. Cai, et al., Breast Cancer Diagnosis by Convolutional Neural Network and Advanced Thermal Exchange Optimization Algorithm, Comput. Math. Methods Med. 2021 (2021).
[11] W. Cai, et al., Optimal bidding and offering strategies of compressed air energy storage: A hybrid robust-stochastic approach, Renew. Energy 143 (2019) 1–8.
[12] S. Manoharan, Early diagnosis of lung cancer with probability of malignancy calculation and automatic segmentation of lung CT scan images, Journal of Innovative Image Processing (JIIP) 2 (04) (2020) 175–186.
[13] A.R. Larici, et al., Lung nodules: size still matters, Eur. Respir. Rev. 26 (146) (2017).
[14] S. Lakshmanaprabu, et al., Optimal deep learning model for classification of lung cancer on CT images, Futur. Gener. Comput. Syst. 92 (2019) 374–382.
[15] SR, S.C. and H. Rajaguru, *Lung cancer detection using probabilistic neural network with modified crow-search algorithm.* Asian Pacific Journal of Cancer Prevention, 2019. **20**(7): p. 2159-2166.
[16] P.M. Shakeel, et al., Automatic detection of lung cancer from biomedical data set using discrete AdaBoost optimized ensemble learning generalized neural networks, Neural Comput. & Applic. 32 (3) (2020) 777–790.
[17] M. Toğaçar, B. Ergen, Z. Cömert, Detection of lung cancer on chest CT images using minimum redundancy maximum relevance feature selection method with convolutional neural networks, Biocybern. Biomed. Eng. 40 (1) (2020) 23–39.
[18] alyasriy, h. *IQ-OTH/NCCD - Lung Cancer Dataset*. 2020; Available from: https://www.kaggle.com/datasets/adityamahimkar/iqothnccd-lung-cancer-dataset.
[19] N. Razmjooy, et al., *Computer-Aided Diagnosis of Skin Cancer: A Review*. Current Medical, Imaging (2020).
[20] Q. Liu, et al., Computer-aided breast cancer diagnosis based on image segmentation and interval analysis, Automatika 61 (3) (2020) 496–506.
[21] R. Ranjbarzadeh, et al., Nerve optic segmentation in CT images using a deep learning model and a texture descriptor, Complex Intell. Syst. (2022) 1–15.
[22] M.B. Umair, et al., A Network Intrusion Detection System Using Hybrid Multilayer Deep Learning Model, Big Data (2022).
[23] M. Makaremi, N. Razmjooy, M. Ramezani, A new method for detecting texture defects based on modified local binary pattern, SIViP 12 (7) (2018) 1395–1401.
[24] N. Razmjooy, V.V. Estrela, H.J. Loschi, Entropy-Based Breast Cancer Detection in Digital Mammograms Using World Cup Optimization Algorithm, International Journal of Swarm Intelligence Research (IJSIR) 11 (3) (2020) 1–18.
[25] A. Hu, N. Razmjooy, Brain tumor diagnosis based on metaheuristics and deep learning, Int. J. Imaging Syst. Technol. 31 (2) (2021) 657–669.
[26] S.-C. Huang, F.-C. Cheng, Y.-S. Chiu, Efficient contrast enhancement using adaptive gamma correction with weighting distribution, IEEE Trans. Image Process. 22 (3) (2013) 1032–1041.
[27] M. Ghiasi, et al., A comprehensive review of cyber-attacks and defense mechanisms for improving security in smart grid energy systems: Past, present and future, Electr. Pow. Syst. Res. 215 (2023), 108975.
[28] N. Ghadimi, et al., An innovative technique for optimization and sensitivity analysis of a PV/DG/BESS based on converged Henry gas solubility optimizer: A case study, IET Gener. Transm. Distrib. (2023).
[29] M. Mir, et al., Application of hybrid forecast engine based intelligent algorithm and feature selection for wind signal prediction, Evol. Syst. 11 (4) (2020) 559–573.
[30] F. Mirzapour, et al., A new prediction model of battery and wind-solar output in hybrid power system, J. Ambient Intell. Hum. Comput. 10 (1) (2019) 77–87.
[31] M. Saeedi, et al., Robust optimization based optimal chiller loading under cooling demand uncertainty, Appl. Therm. Eng. 148 (2019) 1081–1091.
[32] M. Ghiasi, et al., Evolution of smart grids towards the Internet of energy: Concept and essential components for deep decarbonisation, IET Smart Grid 6 (1) (2023) 86–102.
[33] M.T. Hagh, H. Ebrahimian, N. Ghadimi, Hybrid intelligent water drop bundled wavelet neural network to solve the islanding detection by inverter-based DG, Frontiers in Energy 9 (1) (2015) 75–90.
[34] S.-H. Wang, et al., Alcoholism detection by data augmentation and convolutional neural network with stochastic pooling, J. Med. Syst. 42 (2018) 1–11.
[35] A. Alferaidi, et al., Distributed Deep CNN-LSTM Model for Intrusion Detection Method in IoT-Based Vehicles, Math. Probl. Eng. 2022 (2022).
[36] Y.-D. Zhang, et al., Abnormal breast identification by nine-layer convolutional neural network with parametric rectified linear unit and rank-based stochastic pooling, Journal of computational science 27 (2018) 57–68.
[37] N. Ghadimi, et al., SqueezeNet for the forecasting of the energy demand using a combined version of the sewing training-based optimization algorithm, Heliyon (2023).
[38] D. Yu, et al., Energy management of wind-PV-storage-grid based large electricity consumer using robust optimization technique, J. Storage Mater. 27 (2020), 101054.
[39] B. Liu, et al., Improved particle swarm optimization combined with chaos, Chaos, Solitons & Fractals 25 (5) (2005) 1261–1271.
[40] M. Jain, V. Singh, A. Rani, A novel nature-inspired algorithm for optimization: Squirrel search algorithm, Swarm Evol. Comput. 44 (2019) 148–175.
[41] W. Zhao, L. Wang, Z. Zhang, Supply-demand-based optimization: a novel economics-inspired algorithm for global optimization, IEEE Access 7 (2019) 73182–73206.
[42] D. Simon, Biogeography-based optimization, IEEE Trans. Evol. Comput. 12 (6) (2008) 702–713.
[43] F.A. Hashim, A.G. Hussien, Snake Optimizer: A novel meta-heuristic optimization algorithm, Knowl.-Based Syst. 242 (2022), 108320.
[44] E. Han, N. Ghadimi, Model identification of proton-exchange membrane fuel cells based on a hybrid convolutional neural network and extreme learning machine optimized by improved honey badger algorithm, Sustainable Energy Technol. Assess. 52 (2022), 102005.
[45] N. Razmjooy, et al., A comprehensive survey of new meta-heuristic algorithms. Recent Advances in Hybrid Metaheuristics for Data Clustering, Wiley Publishing, 2019.
[46] M.F. Abdullah, et al., Classification of Lung Cancer Stages From CT Scan Images Using Image Processing and K-Nearest Neighbours, IEEE, 2020.
[47] M.A. Khan, et al., Lungs cancer classification from CT images: An integrated design of contrast based classical features fusion and selection, Pattern Recogn. Lett. 129 (2020) 77–85.
[48] X. Wang, et al., Weakly supervised deep learning for whole slide lung cancer image analysis, IEEE Trans. Cybern. 50 (9) (2019) 3950–3962.
[49] A. Kumar, et al., Co-learning feature fusion maps from PET-CT images of lung cancer, IEEE Trans. Med. Imaging 39 (1) (2019) 204–217.
[50] W.J. Sori, et al., DFD-Net: lung cancer detection from denoised CT scan image using deep learning, Front. Comp. Sci. 15 (2) (2021) 1–13.